

# Spatiotemporal seismicity pattern of the Taiwan orogen

Yi-Ying Wen<sup>1,2\*</sup>, Chien-Chih Chen<sup>3,4</sup>, Strong Wen<sup>1,2</sup>, and Wei-Tsen Lu<sup>1</sup>

<sup>1</sup>Department of Earth and Environmental Sciences, National Chung Cheng University,  
Chia-yi County 62102, Taiwan

<sup>2</sup>Environment and Disaster Monitoring Center, National Chung Cheng University,  
Chia-yi County 62102, Taiwan

<sup>3</sup>Department of Earth Sciences, National Central University, Taoyuan City 32001,  
Taiwan

<sup>4</sup>Earthquake-Disaster & Risk Evaluation and Management Center, National Central  
University, Taoyuan City 32001, Taiwan

**Correspondence:** Yi-Ying Wen ([yyyingwen@ccu.edu.tw](mailto:yyyingwen@ccu.edu.tw))

## Abstract

We investigate the temporal and spatial seismicity patterns prior to eight  $M > 6$  events nucleating in different regions of Taiwan through a region-time-length algorithm and an analysis of a self-organizing spinodal model. Our results ~~show~~reveal that the spatiotemporal seismicity variations during the preparation process of impending earthquakes display distinctive patterns corresponding to tectonic settings. Q-type events occur in southern Taiwan and experience a seismic quiescence stage prior to the mainshock. A seismicity decrease of  $2.5 < M < 4.5$  events occurs around the relatively high b-value southern Central Range, which contributes to the accumulation of tectonic stress for preparing for the occurrence of the Q-type event. On the other hand, A-type events occur in central Taiwan and experience a seismic activation stage prior to the mainshock, which nucleates on the edge of the seismic activation area. We should consider when accelerating seismicity of  $3 < M < 5$  events appears within the low b-value area, which could promote the nucleation process of the A-type event.

## 30 1. Introduction

31 Seismic activity is related to spatiotemporal variations in the stress field and state,  
32 and seismicity changes prior to a large earthquake have been widely observed through  
33 different techniques, e.g., b-value analysis (Chan et al., 2012; Wyss and Stefansson,  
34 2006), noncritical precursory accelerating seismicity theory (PAST) (Mignan and  
35 Giovambattista, 2008), pattern informatics (PI) algorithm (Rundle et al., 2003; Chen et  
36 al., 2005), the region-time-length (RTL) algorithm (Chen and Wu, 2006; Wen et al.,  
37 2016), and the analysis of self-organizing spinodal (SOS) model (Rundle et al., 2000).  
38 Previous studies have mostly focused on a significant earthquake; therefore, it is not  
39 easy to understand whether the properties of seismic activation and quiescence patterns  
40 respond to regional tectonic stress.

41 The Taiwan orogenic belt, which is an active and ongoing arc–continent collision  
42 zone as a result of the Philippine Sea Plate (PSP) obliquely colliding with the Eurasian  
43 Plate (EP), is particularly complex due to the two adjacent subduction zones, the  
44 Ryukyu trench and Manila trench to the northeast and south of the island, respectively  
45 (Suppe, 1984; Yu et al., 1997). The frequent and significant seismic activities as well  
46 as a rapid convergence rate of 85 to 90 mm/yr are well observed by the island-wide  
47 GPS and seismic networks (Fig. 1). ~~Suppe (1984) pointed out that the~~The growth of the  
48 Taiwan orogenic belt shows propagation from north to south due to oblique plate  
49 convergence and opposing subduction in the southern and northern parts of Taiwan  
50 (Suppe, 1984). The central part of Taiwan, which is experiencing rapid to full collision,  
51 mainly consists of the Coastal Range, Central Range and Western Foothills (Shyu et al.,  
52 2005a; b). A myriad of active and thin-skinned structures are the products of the  
53 accretion of the continental sliver to the continental margin. In southern Taiwan, the EP  
54 subducting eastward beneath the PSP is in a stage of incipient arc–continent collision

55 (Kao et al., 2000; Shyu et al., 2005a; b). The northwest domain of southern  
56 Taiwan coastal plain and foothill region, which represent the southern tip of the fold-  
57 and-thrust belt in the coastal plain and foothill region in western Taiwan and show very  
58 low seismicity, mainly consist of Miocene shallow marine deposits and a Pliocene–  
59 Pleistocene foreland basin as well as mudstones. ~~On the other hand, the southern~~  
60 ~~Central Range is mainly composed of Oligocene to Miocene metamorphic slates and~~  
61 ~~contains ductile folds and cleavages as well as superimposed faults.~~ Central Taiwan,  
62 ~~which is experiencing rapid to full collision, mainly consists of the Coastal Range,~~  
63 ~~Central Range and Western Foothills (Shyu et al., 2005).~~

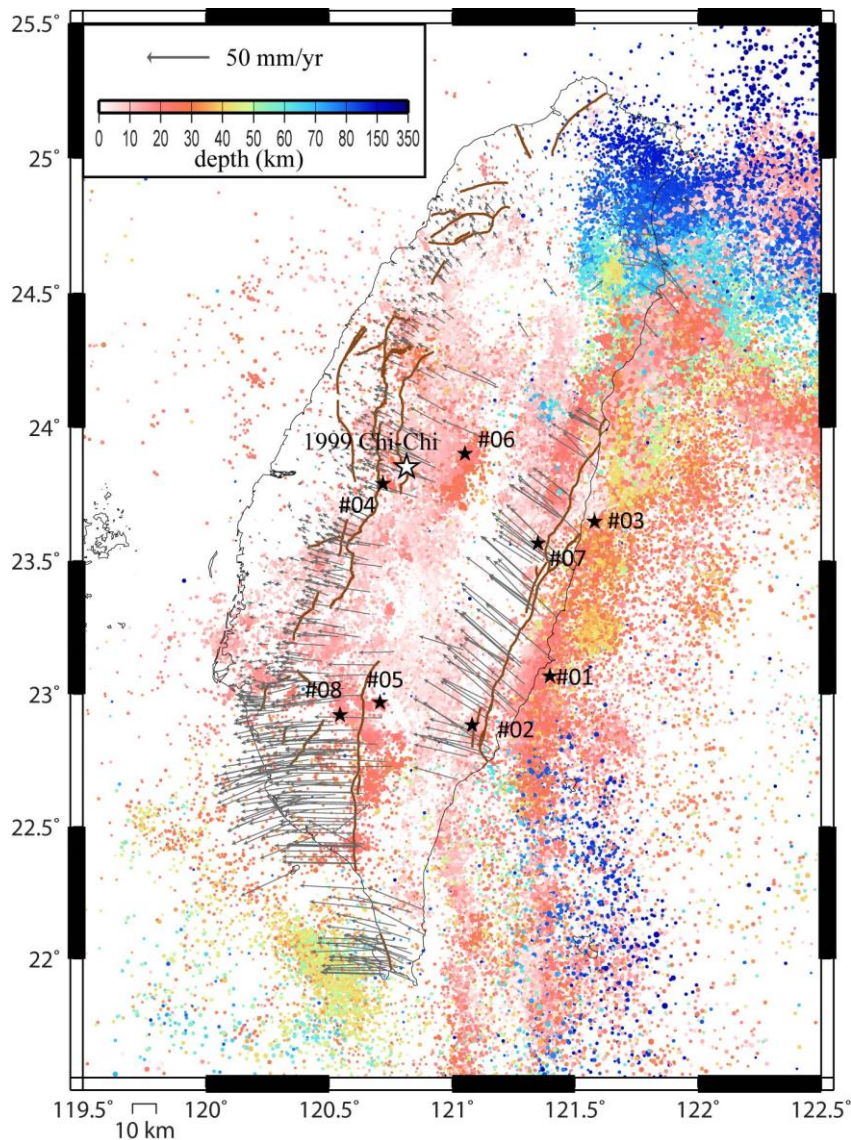


**Figure 1:** Horizontal velocities from 2002 to 2017 (Chen et al., 2018) and seismicity between 1991 and 2018. The white star shows the location of the 1999 Chi-Chi earthquake, and the black stars represent the locations of the investigated events in this study. The active faults (thick lines) identified by the Central Geological Survey of Taiwan are also shown.

64

65 ~~A myriad of active and thin-skinned structures are the products of the accretion of the~~  
 66 ~~continental sliver to the continental margin.~~ Over the last two decades, several moderate  
 67 earthquakes have occurred with various seismicity patterns and in GPS velocity field  
 68 regions. We investigate the temporal and spatial seismicity patterns prior to eight  $M > 6$   
 69 events nucleated in different regions of Taiwan through the RTL algorithm and analysis  
 70 of the SOS model. Our attempt is not to catch the seismic precursor but to focus on the  
 71 seismicity changes related to the regional tectonics, which might become useful hints  
 72 for potential seismic hazard assessments. The results ~~reveal~~ show that the temporal and  
 73 spatial seismicity ( $2.5 < M < 5$ ) variations during the preparation process of impending  
 74 earthquakes could display distinctive patterns corresponding to the tectonic setting.

75

## 76 2. RTL Algorithm and Data

77 The region-time-length (RTL) algorithm (Sobolev and Tyupkin, 1997; 1999) is a  
 78 statistical technique to detect the occurrence of seismic quiescence and activation by  
 79 taking into account the location, occurrence time and magnitude of earthquakes. The  
 80 RTL value is defined as the product of the three dimensionless factors,  $R$ ,  $T$  and  $L$ :

$$81 \quad R(x, y, z, t) = \left[ \sum_{i=1}^n \exp\left(-\frac{r_i}{r_0}\right) \right] - R_{bk}(x, y, z, t) \quad (1)$$

$$82 \quad T(x, y, z, t) = \left[ \sum_{i=1}^n \exp\left(-\frac{t-t_i}{t_0}\right) \right] - T_{bk}(x, y, z, t) \quad (2)$$

$$83 \quad L(x, y, z, t) = \left[ \sum_{i=1}^n \left(\frac{l_i}{r_i}\right) \right] - L_{bk}(x, y, z, t) \quad (3)$$

84 where  $r_i$  is the distance between the investigated point  $(x, y, z)$  and the  $i$ th prior  
 85 event (with the occurrence time  $t_i$  and rupture length  $l_i$ ).  $n$  is the number of prior events

86 that occurred in a defined space–time window with  $r_i \leq 2r_0$  ( $r_0$ , characteristic distance)  
87 and  $(t - t_i) \leq 2t_0$  ( $t_0$ , characteristic time-span). Rupture length  $l_i$  is a function of  
88 earthquake magnitude ( $M_i$ ),  $\log l_i = 0.5M_i - 1.8$  (Kasahara, 1981). The weighted RTL  
89 value reflects the deviation from the background seismicity level ( $R_{bk}$ ,  $T_{bk}$  and  $L_{bk}$ ) with  
90 negative values for seismic quiescence and positive values for activation.  $r_0$   
91 characterizes the decreasing influence of more distant events, and  $t_0$  describes the  
92 reducing influence rate of the preceding events as the time of calculation moving on.  
93 To diminish the ambiguity in determining the characteristic parameters, we follow the  
94 systematic procedure of correlation analysis over pairs of RTL results proposed by  
95 Huang and Ding (2012) to obtain the optimal model parameters,  $\tilde{r}_0$  and  $\tilde{t}_0$ , of each  
96 event. Details of this technique of correlation analysis are described in Appendix A. We  
97 calculate various combinations of  $r_0$  (ranging between 25 and 80 km with a step of 2.5  
98 km) and  $t_0$  (ranging between 0.25 and 2.0 yr with a step of 0.05 yr). As the correlation  
99 coefficient criterion  $C_0$  is set, we can calculate the ratio  $W$  (or weight) of the  
100 combination with correlation coefficients equal to or larger than  $C_0$  for each model  
101 parameter of  $r_{0i}$  ( $i=1\sim m$ ;  $m=23$ ) and  $t_{0j}$  ( $j=1\sim n$ ;  $n=36$ ).

102 After testing many criterion sets, the criterion coefficient  $C_0 = 0.6$  and criterion  
103 ratio  $W_0 = 0.5$  are acceptable for each event, which represents at least 50% of the total  
104 combination pairs with correlation coefficient  $C \geq C_0 = 0.6$ . Then, we obtain the average  
105  $\tilde{r}_0 = 49.6$  km and average  $\tilde{t}_0 = 1.16$  yr. These model parameters are similar to those of  
106 previous studies for Taiwan (Chen and Wu, 2006; Wen et al., 2016; Lu, 2017; Wen and  
107 Chen, 2017).

108 For statistical analyses, catalog completeness is an important factor. Since 1991,  
109 the Taiwan Telemetered Seismographic Network (TTSN) (Wang, 1989) has merged  
110 with the Central Weather Bureau (CWB) seismic network and updated to an integrated

111 earthquake observation system, named the Central Weather Bureau Seismic Network  
112 (CWBSN). Wang et al. (1994) pointed out that most shallow earthquakes occurring in  
113 Taiwan are distributed at depths less than 35 km. According to previous studies (Wu  
114 and Chiao, 2006; Wu et al., 2008; Wen et al., 2016; Hsu et al., 2021), we used the  
115 earthquake catalog maintained by the CWB for the entire Taiwan area with  $M \geq 2.5$  and  
116  $\text{depth} \leq 35$  km between 1991 and 2018 and applied a declustering procedure proposed  
117 by Gardner and Knopoff (1974). Considering a sufficient background seismicity and  
118 minimizing the influence of the 1999 Chi-Chi earthquake, we only selected the  $M > 6$   
119 inland earthquakes between 2003 and 2016 in Taiwan. Since two events occurring in a  
120 close space–time window would show high similarity in RTL function (Lu, 2017), we  
121 neglected the event occurring within  $2\tilde{t}_0$  and  $\tilde{r}_0$  with respect to the last  $M > 6$  events. For  
122 example, two  $M > 6$  events within a distance of 10 km struck the Nantou area on 27  
123 March 2013 and 02 June 2013, and we only analyzed the former event. Therefore, we  
124 have eight qualified  $M > 6$  events, as listed in Table 1.

125

126 **Table 1:** Earthquake parameters for the investigated events determined by the CWB.

No.	Date (UT)	Long. (deg.)	Lat. (deg.)	Depth (km)	$M_L$
1	2003/12/10 04:38:14	121.398	23.067	17.7	6.4
2	2006/04/01 10:02:20	121.081	22.884	7.2	6.2
3	2009/10/03 17:36:06	121.579	23.648	29.2	6.1
4	2009/11/05 09:32:58	120.719	23.789	24.1	6.2
5	2010/03/04 00:18:52	120.707	22.969	22.6	6.4
6	2013/03/27 02:03:20	121.053	23.902	19.4	6.1
7	2013/10/31 12:02:10	121.349	23.566	15.0	6.4
8	2016/02/05 19:57:26	120.544	22.922	14.6	6.6

127

128

### 129 **3. Results**

#### 130 **3.1 Temporal seismicity variation**

131 The temporal variation in the RTL function represents the different stages of  
132 seismicity rate change at the target location with respect to the background level. For  
133 consistency, we adopt a 10-year catalog as the background for each investigated event.  
134 Figure 2 shows the temporal variation in the RTL functions prior to the investigated  
135 events. We can see that before the occurrence of the investigated event, both seismicity  
136 changes are observed: the seismic quiescence stage for Nos. 1, 2, 5 and 8 (Q-type events  
137 hereafter) and the seismic activation stage for Nos. 3, 4, 6 and 7 (A-type events  
138 hereafter). Q-type events occurred at different locations in southern Taiwan, and most,  
139 3 among 4, of their temporal RTL functions reveal the seismic quiescence stages during  
140 2002–2004, which was before the occurrence of the 2003 Chengkung earthquake, i.e.,  
141 event No. 1. The seismicity increase (activation stage) took approximately two years  
142 following the 2003 Chengkung mainshock (event No. 1). We note that the length of the  
143 seismic quiescence stage prior to the Q-type event might correspond to the magnitude.



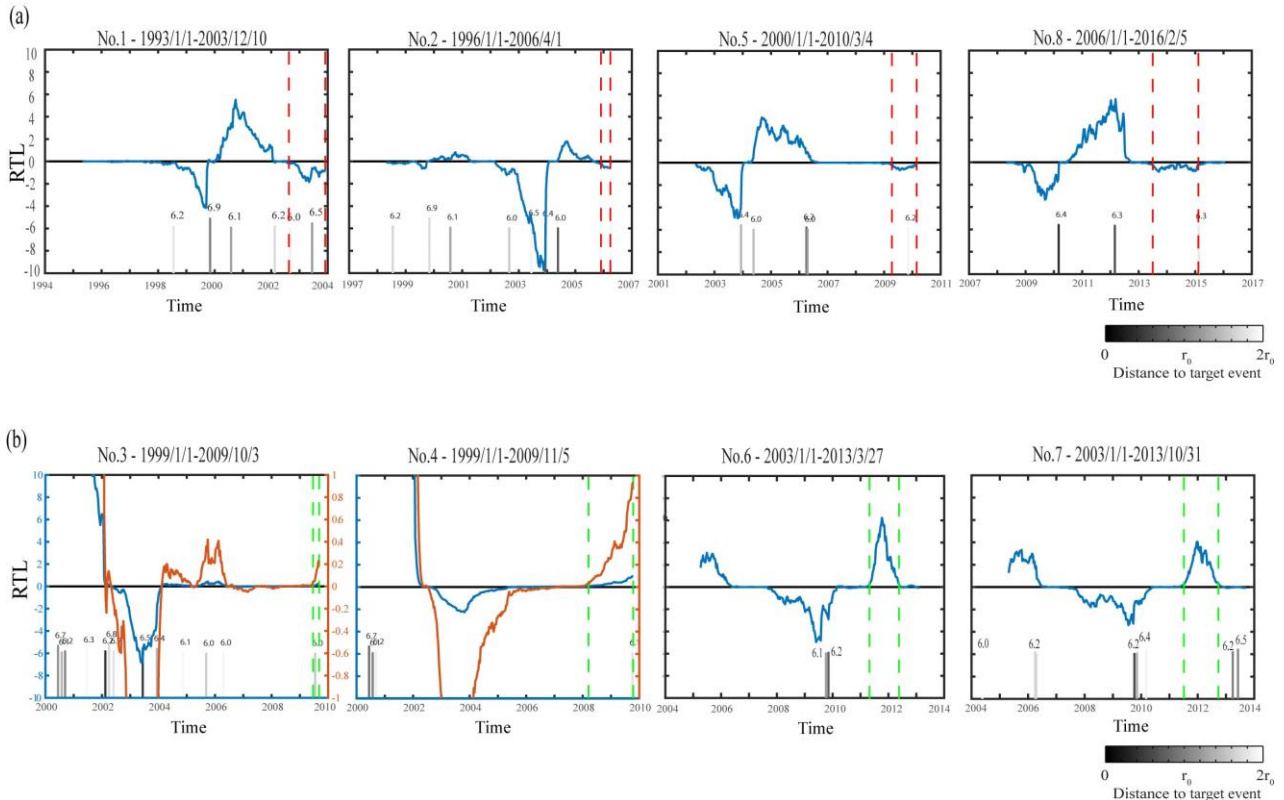


**Figure 2:** Temporal variation of the RTL function (blue line) for (a) Q-type events and (b) A-type events. The orange curves and vertical axes on the right represent the enlarged RTL functions of event Nos. 3 and 4. The vertical dashed red lines mark the seismic quiescence stage, and the vertical dashed green lines mark the seismic activation stage. The bar chart represents the occurrence time of  $M \geq 6.0$  events within a distance of  $2r_0$  from the target event; each number above the bar is the magnitude.

144

145 A-type events all occurred in central Taiwan and were located within  $2\tilde{r}_0$  with respect  
 146 to the 1999 Chi-Chi earthquake. Figure 3 shows the declustered seismicity distribution  
 147 as a function of time and latitude. Significant seismicity followed the 1999 Chi-Chi  
 148 earthquake north of  $23^\circ\text{N}$ . Since the background seismicity of event Nos. 3 and 4 started  
 149 from 1999/01/01, the RTL functions were obviously affected by the occurrence of the  
 150 1999 Chi-Chi earthquake. Therefore, we enlarge the vertical axis to accentuate the  
 151 seismicity variation prior to event Nos. 3 and 4. As shown in Fig. 2, the temporal RTL  
 152 functions of A-type events mostly show a seismic activation stage between 2004 and  
 153 2006, which corresponds to the seismicity increase following the 2003 Chengkung



154 mainshock (event No. 1). However, for the A-type event, we could not see the  
 155 relationship between the length of the seismic activation stage and the magnitude.  
 156

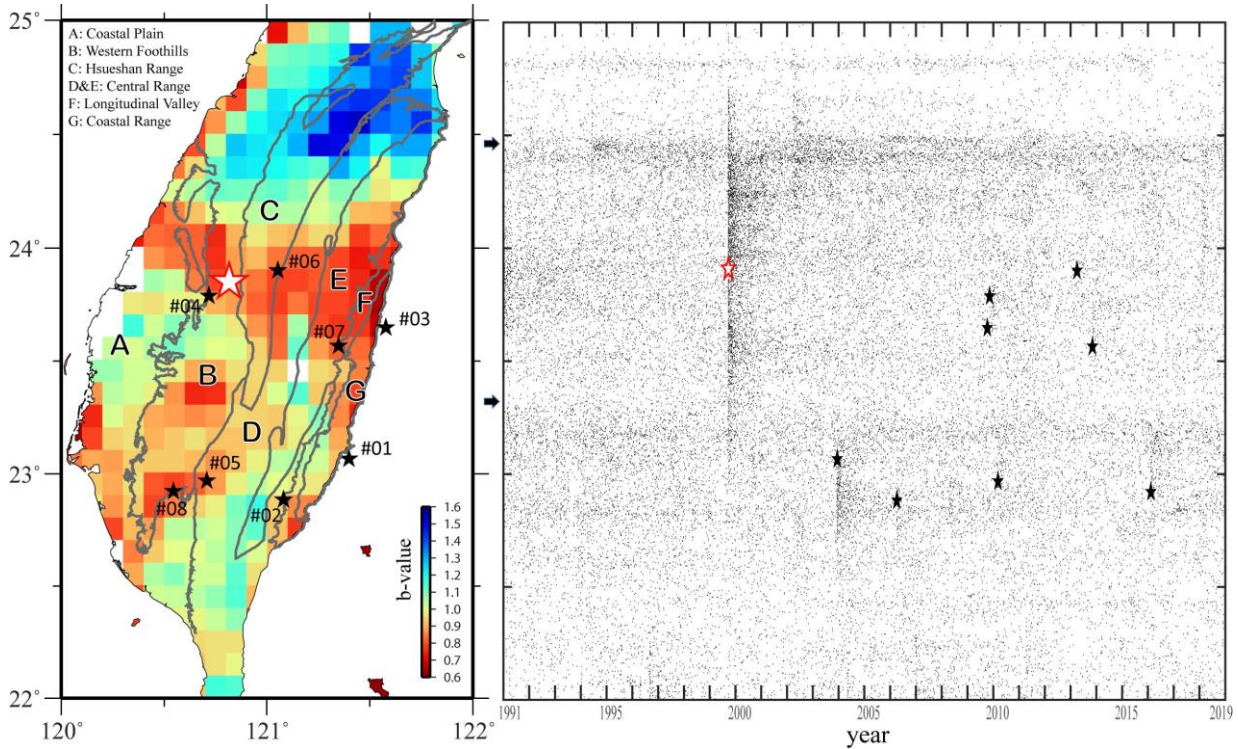


**Figure 3:** Map view of the earthquake b-value and declustered seismicity distribution as a function of time and latitude. The white star indicates the 1999 Chi-Chi earthquake, and the black stars represent the investigated events in this study. The black arrows indicate the seismicity boundaries. The major geological units in Taiwan are marked by gray curves and labeled from A to G. The active faults (thick lines) identified by the Central Geological Survey of Taiwan are also shown.

157

158

### 3.2 Spatial Seismic Activation/Quiescence Distribution

160 Since Q-type and A-type events are located in southern and central Taiwan,  
 161 respectively, it would be worth examining the spatial pattern of their abnormal  
 162 seismicity stages. Wen and Chen (2017) pointed out that various seismic activation or  
 163 quiescence processes of about 2–4 years were found prior to some events occurring in  
 164 Taiwan (Chen and Wu, 2006; Wen et al., 2016; Wu et al., 2008). Thus, for consistency,

165 we only consider the last abnormal stage within four years prior to the investigated  
166 events, as marked by red vertical lines for the quiescence stage of Q-type events and  
167 green vertical lines for the activation stage of A-type events. Then, we calculate the  
168 summation of the selected period to generate the seismic quiescence/activation  
169 distribution. Considering the definition of the weighted RTL function, a sufficient  
170 amount of background seismicity should be regarded as a criterion (Wen and Chen,  
171 2017). Using the declustered catalog from 1991 to 2016, we set up two conditions  
172 similar to those of Wen and Chen (2017) for each grid to strengthen the reliability: (i)  
173 the total number of events within the grid area of  $0.1^\circ \times 0.1^\circ$  must be more than 26 (i.e.,  
174 at least 1 event occurred every year on average); and (ii) the total events within a circle  
175 of  $2r_0$  in radius must be more than 9360 (i.e., at least 30 events occurred every month  
176 on average). For each event, we normalize the spatial distribution based on the summed  
177 result. The spatial seismic activation/quiescence map provides the information of  
178 influence of surrounding seismicity state to the target event during the abnormal stage.  
179 Similar to previous studies (e.g., Huang et al., 2001; Huang and Ding, 2012), Fig. 4  
180 shows that Q-type events mostly occurred on the edge of the seismic quiescence area;  
181 and seismic activation appeared around A-type events ~~occurred on the edge of the~~  
182 ~~seismic activation area.~~

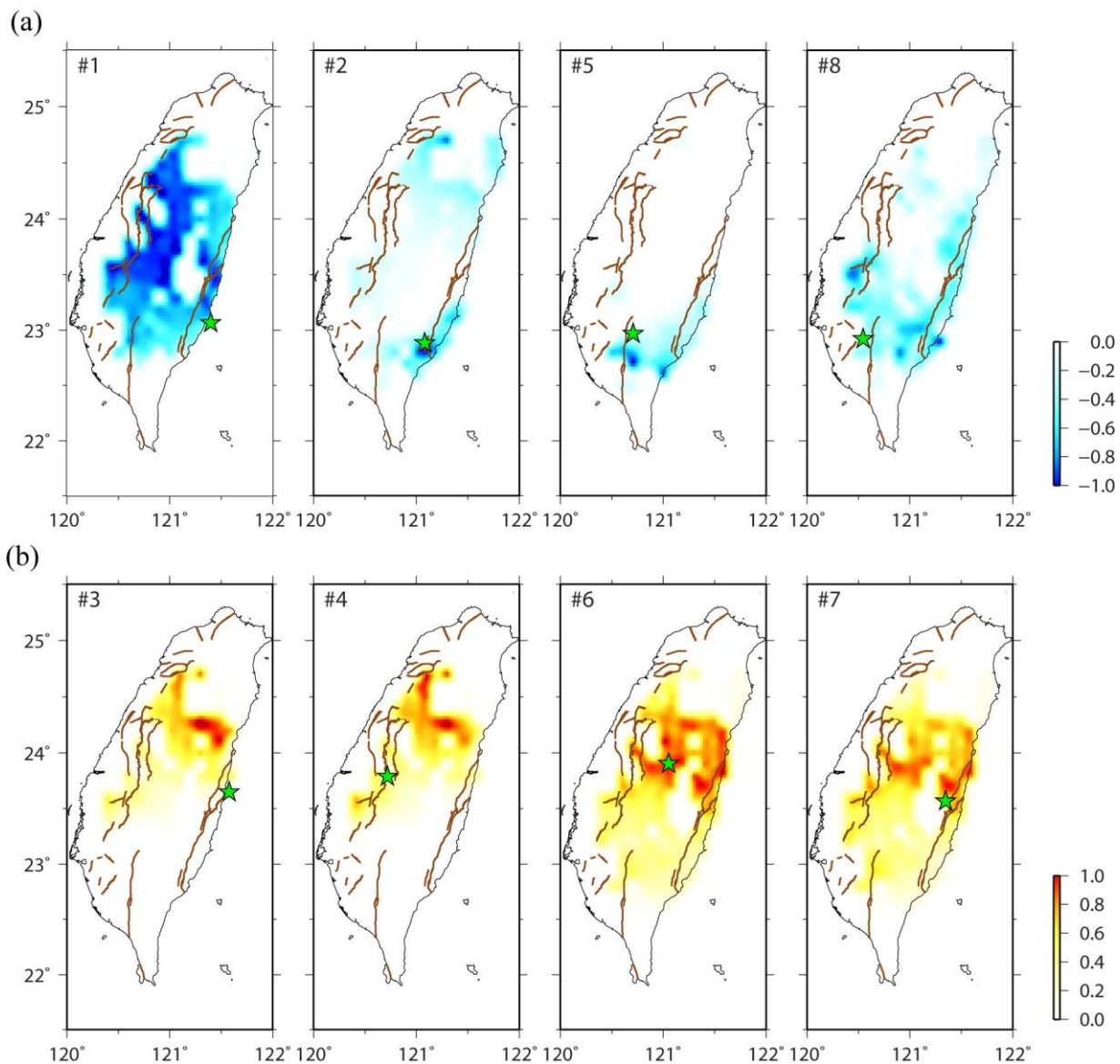


**Figure 4:** (a) The summed and normalized seismic quiescence map for the selected time window of the temporal RTL function of Q-type events, and (b) the summed and normalized seismic activation map for the selected time window of the temporal RTL function of A-type events. Stars represent the locations of the investigated events. The active faults (thick lines) identified by the Central Geological Survey of Taiwan are also shown.

183

## 184 4. Discussion

### 185 4.1 Spatiotemporal Characteristics of Seismicity Changes

186 The RTL analysis accounts for the background seismicity prior to the investigated

187 event. ~~For example, the analysis for event No. 1 (i.e., the 2003 Chengkung earthquake)~~

188 ~~used the declustered catalog between 1993/01/01 and 2003/12/09 as background~~

189 ~~seismicity for each grid. Four A-type events occurred in two different years: event Nos.~~  
190 ~~3 and 4 in 2009 and event Nos. 6 and 7 in 2013 (Fig. 2).~~ Therefore, the RTL analyses  
191 account for almost the same background length for event Nos. 3 and 4 (1999-2009) and  
192 for event Nos. 6 and 7 (2003-2013), respectively. As the temporal RTL functions show  
193 the seismic activation stage prior to the mainshocks during a similar period, we could  
194 expect similar seismic activation maps for event Nos. 3 versus 4 and event Nos. 6 versus  
195 7, as shown in Fig. 4. Furthermore, the seismic quiescence stage of event No. 5 occurred  
196 in a similar period as the seismic activation stage of event No. 3 (Fig. 2), and the seismic  
197 quiescence area of event No. 5 complements the seismic activation area of event No. 3  
198 (Fig. 4). In contrast, although event Nos. 3 and 7 occurred at close locations, the  
199 difference in the 10-year background period~~4-year background seismicity~~ affects the  
200 weighting of the deviation. For example, ~~as shown in Fig. 2,~~ the seismic quiescence  
201 stage during 2007–2009 ~~shown~~revealed in the temporal RTL function of event No. 7  
202 (Fig. 2) is evaluated as the background seismicity level (RTL value is equal to zero) in  
203 the temporal RTL function with respect to event No. 3. On the other hand, Wen and  
204 Chen (2017) pointed out that an abnormal seismic stage ~~derived~~revealed with various  
205 background periods cannot be produced by chance. The temporal RTL functions of five  
206 events (Nos. 1–5 in Fig. 2) accounting for different background periods all ~~exhibit~~reveal  
207 the seismic quiescence stage before the occurrence of event No. 1. This phenomenon is  
208 consistent with the seismic quiescence map of event No. 1 (Fig. 4) and the Z-value map  
209 of Wu et al. (2008) in which the seismic activity decreased during 2002–2003 for a  
210 large area in Taiwan. In addition, the widespread seismic activation distribution of Nos.  
211 6 and 7 (Fig. 4) also responded to the seismic activity increase during 2011–2012 (Nos.  
212 6–8 in Fig. 2). ~~Overall, the seismic quiescence and activation maps show some~~  
213 ~~characteristics: (i) the seismicity decrease was revealed in the southern Central Range~~

214 ~~prior to the Q-type mainshocks; and (ii) the boundaries appear at approximately 23.2°N~~  
215 ~~and 24.5°N for the abnormal seismicity distributions, which coincide with the~~  
216 ~~distribution of declustered seismicity in Fig. 3.~~

217 Rundle et al. (2000) proposed the self-organizing spinodal (SOS) model for  
218 characteristic earthquakes and suggested that small earthquakes occurred uniformly at  
219 all times, while the occurrence rate of intermediate-sized earthquakes varied during the  
220 earthquake cycle. Chen (2003) investigated the SOS behavior of the 1999 Chi-Chi  
221 earthquake and ~~proposed~~revealed the seismic activation of moderate-size ( $5 < M < 6$ )  
222 events prior to the mainshock. Here, we also calculate the cumulative frequency–  
223 magnitude distributions for these eight events using the same catalog periods of the  
224 RTL analysis. For each investigated event, we only compared the distribution diagrams  
225 of the long-term (background period) and abnormal seismic stages marked by dashed  
226 lines in Fig. 2 within a radius of 25 km with respect to the epicenter. As shown in Fig.  
227 5, cumulative frequency-magnitude distributions of long-term seismicity (red dots)  
228 generally exhibit linear power law distributions. For the Q-type events, the cumulative  
229 frequency distributions of the seismic quiescence stage (black dots) appear to lack  
230  $2.5 < M < 4.5$  events (Fig. 5a), and the lack of a level corresponds to the seismic  
231 quiescence distribution near the epicenter (Fig. 4). This indicates that within the seismic  
232 quiescence stage before the occurrence of the Q-type event, the quiescence of  
233  $2.5 < M < 4.5$  activity contributes to the accumulation of tectonic stress.



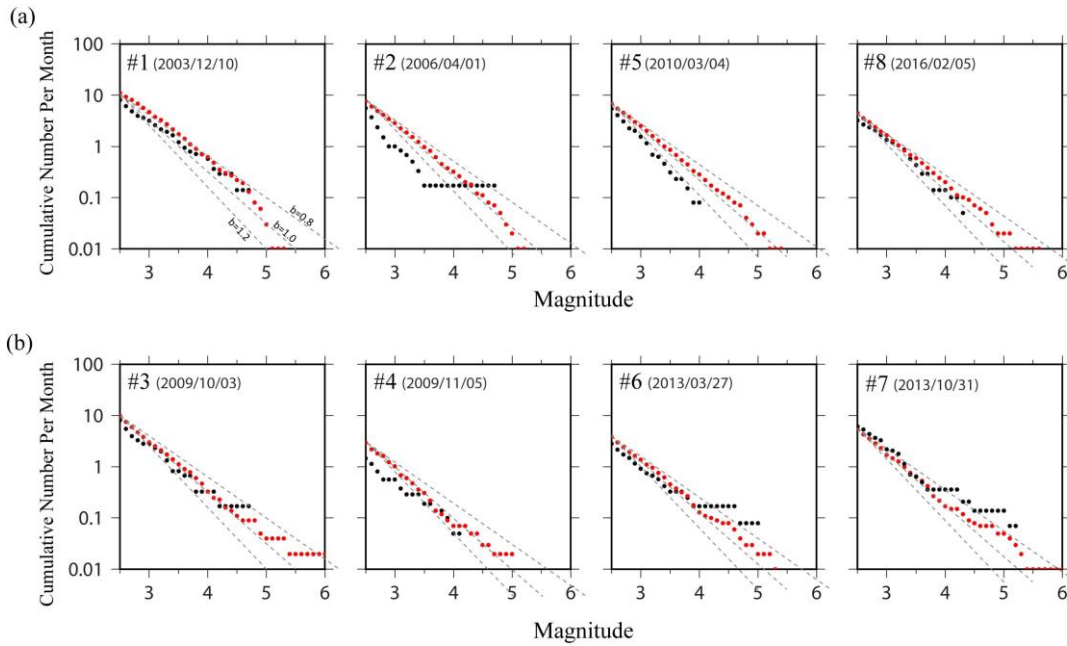


**Figure 5:** The cumulative frequency–magnitude distributions prior to the investigated events. Red and black dots represent the long-term and abnormal seismic stage marked in Fig. 2, respectively.

234

235 On the other hand, the cumulative frequency distributions of the seismic activation  
 236 stage of the A-type events (black dots in Fig. 5b) show that the seismic activation of  
 237  $3 < M < 5$  events within the seismic activation stage before the occurrence of the A-type  
 238 earthquake can be found, which is similar to the results of the 1999 Chi-Chi earthquake  
 239 (Chen, 2003). Event Nos. 6 and 7, which are located very close to the high seismic  
 240 activation area (Fig. 4), display an obvious increase in the number of  $4 < M < 5$  events  
 241 during the seismic activation stage (Fig. 5b).

242 Event No. 4 occurred only one month later than event No. 3; however, the seismic  
 243 activation stage of event No. 4 was much longer than that of event No. 3. Furthermore,  
 244 the cumulative frequency distributions of the seismic activation stage of event No. 4  
 245 display a lower intercept (Fig. 5b), which represents the overall decreasing seismicity  
 246 within this seismic activation stage (Fig. 5b). Here, we further divide the seismic  
 247 activation stage of event No. 4 into three periods for discussion: (i) P1: 2008/02–  
 248 2009/03 before the seismic activation stage of event No. 3; (ii) P2: 2009/04–2009/09

249 matching the seismic activation stage of event No. 3; and (iii) P3: 2009/10 between the  
 250 occurrences of event Nos. 3 and 4. The seismic activation distributions in Fig. 6 are all  
 251 normalized with respect to the maximum RTL value of the seismic activation  
 252 distribution of event No. 4 through Periods P1–P3. We can see that before the seismic  
 253 activation stage of event No. 3 during 2008/02–2009/03 (P1), the location of event No.  
 254 3 indeed shows no seismic activation, as ~~exhibited~~~~revealed~~ in the temporal RTL  
 255 function (Fig. 2b). On the other hand, for the location of event No. 4, the seismic  
 256 activation remains through all three Periods P1–P3. Combined with the overall  
 257 decreasing seismicity indicated by the lower intercept in Fig. 5(b), these results suggest  
 258 that this seismic activation prior to event No. 4 was mainly contributed by the relatively  
 259 accelerating activity of  $3.5 < M < 4$  events.

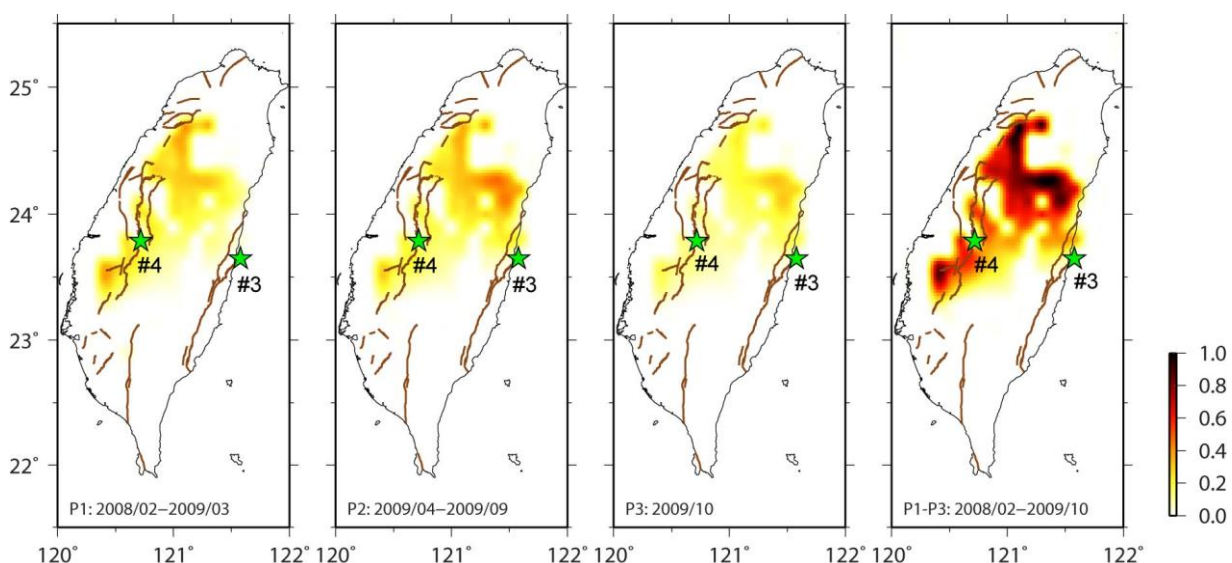


**Figure 6:** The summed seismic activation map for different periods of the seismic activation stage prior to event No. 4; all maps are normalized based on the summed results of P1–P3. Stars represent the locations of event Nos. 3 and 4. The active faults (thick lines) identified by the Central Geological Survey of Taiwan are also shown.

260

## 261 4.2 Implication for the Tectonic Setting

262 Several major active faults in ~~southwestern~~~~southern~~ Taiwan have been identified,  
 263 and most of them have been dominated by thrust movement. Some strike-slip structures,



264 e.g., the Zuo Chen and Hsinhua faults, acted as the transfer structures between these  
265 thrust faults (Ching et al., 2011; Deffontaines et al., 1994, 1997; Rau et al., 2012). These  
266 transfer structures develop at approximately 23°N, which is the northern limit of the  
267 Wadati–Benioff zone (Kao et al., 2000) and close to the seismicity boundary indicated  
268 in Figs. ~~32 and 4~~. Geodetic data ~~displayed~~revealed various rates and orientations of  
269 horizontal shortening with rapid uplift rates in southern Taiwan (Fig. 1), which might  
270 be caused by underplating beneath the Central Range sustaining crustal thickening and  
271 exhumation (Simoes et al., 2007). The seismic b-value, which is the relative earthquake  
272 size distribution, can be derived from the Gutenberg–Richter relation (Gutenberg and  
273 Richter, 1944):  $\log N = a - bM$ , where constant  $a$  is related to seismicity and  $N$  is the  
274 number of earthquakes with magnitudes greater than  $M$ . In general, a high b-value  
275 indicates a larger proportion of small events, and a low b-value suggests that large  
276 earthquakes dominate over small ones. Using the same declustered catalog from 1991  
277 to 2018, we search for events within a radius of 25 km with respect to the center of each  
278 grid (0.1°×0.1°). Only for the grids with more than 30 events, we calculate the b-value  
279 using the weighted least-squares fitting method (Shi and Bolt, 1982) and the spatial  
280 distribution of b-values, as shown in Fig. 3. The seismicity in the southern Central  
281 Range is active but shows significant heterogeneity in faulting types (Chen et al., 2017;  
282 Wu et al., 2018), and relatively high b-values suggest the predominance of small  
283 earthquakes in this region (Fig. 3 and red dots in Fig. 5a; Wu et al., 2018). Wen et al.  
284 (2016) found the decreased seismicity and increased Coulomb stress change revealed  
285 the seismicity decrease in the southern Central Range prior to the 2010 Jiashian  
286 earthquake (i.e., event No. 5). ~~The seismicity rate change can be considered a proxy for~~  
287 ~~the stress state change (Dieterich, 1994; Dieterich et al., 2000),~~ and suggested both  
288 variations in Coulomb stress and seismicity rate play important roles in contributing to

289 the nucleation process of impending earthquakes (~~Wen et al., 2016~~). The seismicity rate  
290 change can be considered a proxy for the stress state change (Dieterich, 1994; Dieterich  
291 et al., 2000), and this implies that the quiescence of seismicity contributes to the  
292 accumulation of tectonic stress. Since this relatively high b-value region in the southern  
293 Central Range has been observed to have a seismicity decrease ( $2.5 < M < 4.5$  events)  
294 before the occurrence of Q-type events, it can be an indicator of stress change.

295 Many devastating earthquakes with surface ruptures have occurred in the central  
296 Taiwan~~this region~~, including the 1935 M 7.1 Hsinchu–Taichung earthquake, the 1951  
297 Longitudinal Valley earthquake sequence and the 1999 Chi-Chi earthquake (Lee et al.,  
298 2007; Chen et al., 2008; Lin et al., 2013). Hsu et al. (2009) derived the consistent  
299 orientations of principal strain-rate and crust stress axes in central Taiwan, which  
300 implies that faulting style corresponds to stress buildup accumulating from interseismic  
301 loading. They also pointed out that for central Taiwan, small events tend to surround  
302 the locked fault zone, where major earthquakes might occur, during the interseismic  
303 period. The 1999 Chi-Chi earthquake ruptured the area near the end of the décollement  
304 with a high contraction rate (Dominguez et al., 2003; Hsu et al., 2003; 2009). In addition,  
305 similar to the 1999 Chi-Chi earthquake, the A-type events occurred in the low b-value  
306 area surrounded by small and active events. Chen and Wu (2006) derived the temporal  
307 RTL function of the 1999 Chi-Chi earthquake, showing a pattern similar to that of A-  
308 type events with the activation stage prior to the mainshock. Furthermore, Wu (2006)  
309 calculated the seismic activation map of the 1999 Chi-Chi event and found that the 1999  
310 Chi-Chi mainshock occurred on the edge of the seismic activation area, which is a low  
311 b-value region. This is similar to the seismic activation maps of A-type events, which  
312 display the hot-spot pattern contracting within the low b-value area (Figs. 2-3 and 4).  
313 The nucleation of the A-type mainshock can be attributed to the perturbation of

314 background seismicity ( $3 < M < 5$  events) by the stress state change (Dieterich, 1994;  
315 Dieterich et al., 2000).

316 The cumulative frequency distributions of long-term seismicity in Fig. 5  
317 ~~show~~ reveal a b-value of 0.8–1.0 around these eight events, which is consistent with the  
318 pattern shown in Fig. 3. However, the cumulative frequency distributions of long-term  
319 seismicity exhibit different trends of magnitudes larger than 4.5 for the two types of  
320 events. The seismicity for  $M > 4.5$  events is lower in the area around the Q-type event  
321 but higher in the area around the A-type event. Event Nos. 1, 2, 3 and 7 occurred in  
322 eastern Taiwan with an average GPS velocity of about 60 mm/yr (Fig. 1), and the  
323 cumulative frequency distributions of long-term seismicity display a high intercept (Fig.  
324 5). This rapid convergence rate generally remains in the western part of southern  
325 Taiwan, which indicates that only a little shortening is consumed from east to the west  
326 in southern Taiwan. This corresponds to the active seismicity of small earthquakes, as  
327 ~~indicated~~ revealed by the high intercept of the cumulative frequency distributions of  
328 long-term seismicity for event Nos. 1, 2, 5 and 8 (Fig. 5). Therefore, for the pre-  
329 collisional rapid and distributed convergence in southern Taiwan (Shyu et al.,  
330 2005a), the quiescence of  $2.5 < M < 4.5$  activity contributes to the accumulation of  
331 tectonic stress for preparing for the occurrence of the Q-type event. On the other hand,  
332 the shortening rate is obviously consumed in the mountainous area of central Taiwan.  
333 Therefore, the lowest intercept of the cumulative frequency distributions of long-term  
334 seismicity for event No. 4 (Fig. 5) reflects the slow GPS velocity and low seismicity in  
335 the western part of central Taiwan (Fig. 1). For central Taiwan, small events tend to  
336 surround the locked fault zone of the potential major events during the interseismic  
337 period, and the 1999 Chi-Chi earthquake is the case affected by the accelerating  
338 seismicity of moderate-size events and ruptured the area near the end of the décollement

339 [with a high contraction rate \(Chen, 2003; Dominguez et al., 2003; Hsu et al., 2003;](#)  
340 [2009\)](#). Tectonic stress accumulating from the interseismic loading with the perturbation  
341 of the accelerating activity of  $3 < M < 5$  events could promote the nucleation process of  
342 the A-type event.

343

## 344 5. Conclusion

345 Through statistical analyses of recent large earthquakes that occurred in Taiwan,  
346 we summarize various temporal and spatial seismicity patterns prior to the earthquakes  
347 that nucleated in different regions of Taiwan:

- 348 • Q-type events occurred in southern Taiwan, with the northern boundary of  
349  $23.2^{\circ}\text{N}$ , and experienced a seismic quiescence stage prior to the mainshock.  
350 A seismicity decrease of  $2.5 < M < 4.5$  events in the [relatively](#) high b-value  
351 southern Central Range could be an indicator of stress change related to  
352 the preparation process of such events.
- 353 • A-type events occurred in central Taiwan and experienced a seismic  
354 activation stage prior to the mainshock, which nucleated on the edge of the  
355 seismic activation area. We should consider when accelerating seismicity  
356 of  $3 < M < 5$  events appears within the low b-value area.

357 Our results ~~show~~[reveal](#) that the spatiotemporal seismicity variations during the  
358 preparation process of impending earthquakes could display a distinctive pattern  
359 corresponding to the tectonic setting. However, the mechanisms causing these different  
360 phenomena are not clear, and further study is still needed.

361

362

363 Appendix A

364 In the systematic correlation analysis for searching the optimal model parameters,  
 365 we calculate various combinations of  $r_0$  (ranging between 25 and 80 km with a step of  
 366 2.5 km) and  $t_0$  (ranging between 0.25 and 2.0 yr with a step of 0.05 yr). As the  
 367 correlation coefficient criterion  $C_0$  is set, we can calculate the ratio  $W$  (or weight) of the  
 368 combination with correlation coefficients equal to or larger than  $C_0$  for each model  
 369 parameter of  $r_{0i}$  ( $i=1\sim m$ ;  $m=23$ ) and  $t_{0j}$  ( $j=1\sim n$ ;  $n=36$ ). Then, the contour map for the  
 370 ratio  $W$  is generated, as shown in Fig. A1.

$$371 \quad W_{ij} = \frac{\sum_{k=1}^m I(C_{ik} \geq C_0) + \sum_{l=1}^n I(C_{jl} \geq C_0)}{m+n} \quad (\text{A1})$$

372 where the logical function  $I(\Phi)$  is defined as

$$373 \quad I(\Phi) = \begin{cases} 1, & \Phi \text{ is true} \\ 0, & \text{otherwise} \end{cases} \quad (\text{A2})$$

374 As the criterion ratio  $W_0$  is set, the optimal model parameters,  $\tilde{r}_0$  and  $\tilde{t}_0$ , can be  
 375 obtained by the following formulas:

$$376 \quad \tilde{r}_0 = \frac{\sum_{j=1}^n \sum_{i=1}^m W_{ij} I(W_{ij} \geq W_0) r_{0i}}{\sum_{j=1}^n \sum_{i=1}^m W_{ij} I(W_{ij} \geq W_0)} \quad (\text{A3})$$

$$377 \quad \tilde{t}_0 = \frac{\sum_{i=1}^m \sum_{j=1}^n W_{ij} I(W_{ij} \geq W_0) t_{0j}}{\sum_{i=1}^m \sum_{j=1}^n W_{ij} I(W_{ij} \geq W_0)} \quad (\text{A4})$$

378 Using event No. 6 as an example, we considered criterion coefficient  $C_0 = 0.6$  and  
 379 criterion ratio  $W_0 = 0.5$ , which indicates that at least 50% of the total combination pairs  
 380 had a correlation coefficient  $C \geq C_0 = 0.6$ . Then, we obtained  $\tilde{r}_0 = 50.0$  km and  $\tilde{t}_0 = 1.14$   
 381 yr (diamond in Fig. A1) by averaging the parameter values that passed the criterion.

382 In addition, Nagao et al. (2011) proposed the RTM algorithm to reduce the dual  
 383 effect of the distance ( $r_i$ ) by introducing the new factor

$$384 \quad M(x, y, z, t) = [\sum_{i=1}^n (M_i)] - M_{bk}(x, y, z, t) \quad (\text{A4})$$

385 where  $M_i$  is the earthquake magnitude of the  $i$ th prior event. Here, we also calculate the  
 386 RTM function of each investigated event with the same characteristic parameter set of  
 387 the RTL model, and both functions display very similar trends with minor differences,  
 388 as shown in Figure R2. The reason for this could be that, for these eight events, no large  
 389 earthquakes occurred in the vicinity of the epicenter. The bar chart in Fig. A2, which

390 represents the occurrence time of  $M \geq 6.0$  events within a distance of  $2r_0$  from the target  
 391 event, also supports this explanation.

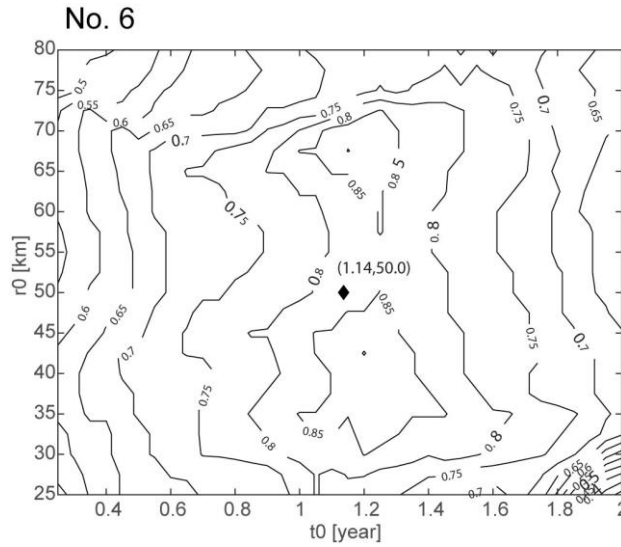


Figure A1: Contour map of ratio  $W$  for various combinations of model parameters of  $r_0$  and  $t_0$ , with  $C_0 = 0.6$  for event No. 6. The diamond shows the optimal model parameters as selecting criterion ratio  $W_0 = 0.5$ .

392  
 393

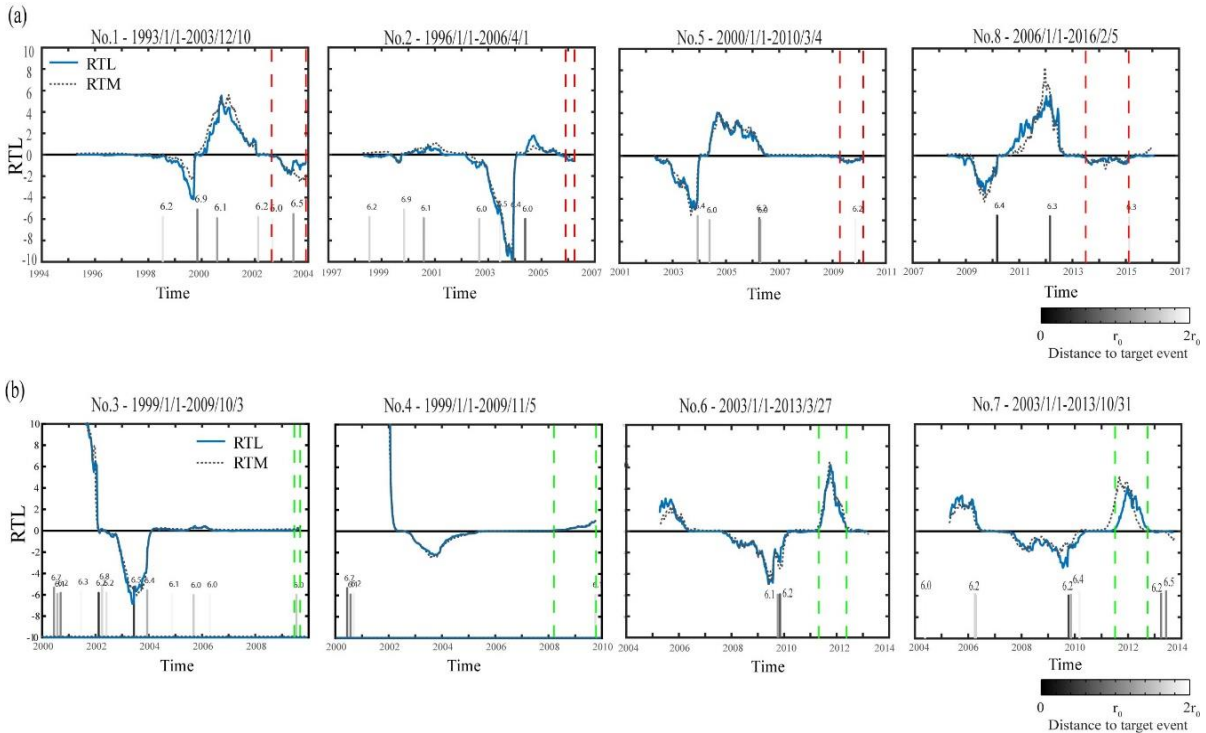


Figure A2: Temporal variation of the RTL (solid line) and RTM (dotted line) functions for (a) A-type events and (b) B-type events. The bar chart represents the occurrence time of  $M \geq 6.0$  events within a distance of  $2r_0$  from the target event; each number above the bar is the magnitude.

394 **Data Availability** : The seismic data is available in the Geophysical Database  
395 Management System (GDMS, <https://gdms.cwb.gov.tw/>). A Chinese manual for data  
396 access from the GDMS is on the website.

397

398 **Author contributions:** Conceptualisation, YYW, CCC; Investigation, YYW, WTL;  
399 Validation, Formal analysis, Writing - original draft preparation, YYW; Writing -  
400 review & editing, YYW, CCC, SW.

401

402 **Competing interests:** The authors declare no conflicts of interest.

403

404 **Acknowledgments:** We thank Central Weather Bureau (CWB) of Taiwan for  
405 providing seismic data. This research was supported by the Ministry of Science and  
406 Technology in Taiwan with grant: MOST 110-2116-M-194-018. The Taiwan  
407 Earthquake Center (TEC) contribution number for this article is \*\*\*\*.

408

409



410 **References:**

- 411 Chan, C.H., Wu, Y.M., Tseng, T.L., Lin, T.L., and Chen, C.C.: Spatial and temporal  
412 evolution of b-values before large earthquakes in Taiwan. *Tectonophysics*, **532**,  
413 215-222, 2012.
- 414 Chen, C.-C., Rundle, J.B., Holliday, J.R., Nanjo, K.Z., Turcotte, D.L., Li, S.C., and  
415 Tiampo, K. F.: The 1999 Chi-Chi, Taiwan, earthquake as a typical example of  
416 seismic activation and quiescence. *Geophys. Res. Lett.*, **32**(22), L22315,  
417 doi:10.1029/2005GL023991, 2005.
- 418 Chen, C.C., and Wu, Y.X.: An improved region–time–length algorithm applied to the  
419 1999 Chi-Chi, Taiwan earthquake. *Geophys. J. Int.*, **166**, 1144-1147, doi  
420 10.1111/j.1365-246X.2006.02975.x, 2006.
- 421 Chen, J.S., Ching, K.E., Rau, R.J., Hu, J.C., Cheng, K.C., Chang, W.L., Chuang, R.Y.,  
422 Chen, C.L., and Chen, H.C.: Surface deformation in Taiwan during 2002-2017  
423 determined from GNSS and precise leveling measurements. Central Geological  
424 Survey Special Publication, 33, 157-178, 2018. (in Chinese with English abstract)
- 425 Chen, K.H., Toda, S., and Rau, R.J.: A leaping, triggered sequence along a segmented  
426 fault: the 1951 Hualien – Taitung earthquake sequence in eastern Taiwan. *J.*  
427 *Geophys. Res.*, **113**, B02304, doi:10.1029/2007JB005048, 2008.
- 428 Chen, S.K., Wu, Y.M., Hsu, Y.J., and Chan, Y.C.: Current crustal deformation  
429 reassessed by cGPS strain-rate estimation and focal mechanism stress inversion.  
430 *Geophys. J. Int.*, **210**, 228–239. <https://doi.org/10.1093/gji/ggx165>, 2017.
- 431 Ching, K.E., Johnson, K.M., Rau, R.J., Chuang, R.Y., Kuo, L.C., and Leu, P.L.:  
432 Inferred fault geometry and slip distribution of the 2010 Jiashian, Taiwan,  
433 earthquake is consistent with a thick-skinned deformation model. *Earth Planet. Sci.*  
434 *Lett.*, EPSL-S-10-00445, doi:10.1016/j.epsl.2010.10.021, 2011.

435 Deffontaines, B., Lee, J.-C., Angelier, J., Carvalho, J., and Rudant, J.-P.: New  
436 geomorphic data on the active Taiwan orogen: a multisource approach. *J. Geophys.*  
437 *Res.*, **99**, 20243–20266, 1994.

438 Deffontaines, B., Lacombe, O., Angelier, J., Mouthereau, F., Lee, C.T., Deramond, J.,  
439 Lee, J.F., Yu, M.S., and Liu, P.M.: Quaternary transfer faulting in Taiwan  
440 Foothills: evidence from a multisource approach. *Tectonophysics*, **274**, 61–82,  
441 1997.

442 Dieterich, J. H.: A constitutive law for rate of earthquake production and its application  
443 to earthquake clustering. *J. Geophys. Res.*, **99** (18), 2601-2618, 1994.

444 Dieterich, J., Cayol, V., and Okubo, P.: The use of earthquake rate changes as a stress  
445 meter at Kilauea volcano. *Nature*, **408**, 457–460, 2000.

446 Dominguez, S., Avouac, J.P., and Michel, R.: Horizontal coseismic deformation of the  
447 1999 Chi-Chi earthquake measured from SPOT satellite images: implications for  
448 the seismic cycle along the western foothills of central Taiwan. *J. Geophys. Res.*,  
449 **108**, doi:10.1029/2001JB000951, 2003.

450 Gardner, J. K., and Knopoff, L.: Is the sequence of earthquakes in Southern California,  
451 with aftershocks removed, Poissonian?. *Bull. Seis. Soc. Am.*, **64**(5), 1363-1367,  
452 1974.

453 Gutenberg, B., and Richter, C.F.: Frequency of earthquakes in California. *Bull. seism.*  
454 *Soc. Am.*, **34**, 185–188, 1944.

455 Hsu, Y.J., Kao, H., Bürgmann, R., Lee, Y.T., Huang, H.H., Hsu, Y.F., and Zhuang, J.:  
456 Synchronized and asynchronous modulation of seismicity by hydrological loading:  
457 A case study in Taiwan. *Sci. Adv.*, **7** (16), p. eabf7282, doi:  
458 10.1126/sciadv.abf7282, 2021.

459 Hsu, Y.J., Simons, M., Yu, S.B., Kuo, L.C., and Chen, H.Y.: A two-dimensional  
460 dislocation model for interseismic deformation of the Taiwan mountain belt. *Earth*  
461 *Planet. Sci. Lett.*, **211**, 287–294, 2003.

462 Hsu, Y.J., Yu, S.B., Simons, M., Kuo, L.C., and Chen, H.Y.: Interseismic crustal  
463 deformation in the Taiwan plate boundary zone revealed by GPS observations,  
464 seismicity, and earthquake focal mechanisms. *Tectonophysics*, **479**, 4–18.  
465 <https://doi.org/10.1016/j.tecto.2008.11.016>, 2009.

466 Huang, Q., and Ding, X.: Spatiotemporal variations of seismic quiescence prior to the  
467 2011 M 9.0 Tohoku earthquake revealed by an improved Region-Time-Length  
468 algorithm. *Bull. Seismol. Soc. Am.*, **102**(4), 1878-1883, doi: 10.1785/0120110343,  
469 2012.

470 Huang, Q., Sobolev, G.A., and Nagao, T.: Characteristics of the seismic quiescence and  
471 activation patterns before the M=7.2 Kobe earthquake. *Tectonophysics*, **337**, 99-  
472 116, 2001.

473 Kao, H., Huang, G.C., and Liu, C.S.: Transition from oblique subduction to collision in  
474 the northern Luzon arc-Taiwan region: Constraints from bathymetry and seismic  
475 observations. *J. Geophys. Res.*, **105**, 3059-3079, 2000.

476 Kasahara, K.: Earthquake Mechanics, *Cambridge Univ. Press., Cambridge*, 248 pp.,  
477 1981.

478 Lee, S.J., Chen, H.W., and Ma, K.F.: Strong Ground Motion Simulation of the 1999  
479 Chi-Chi, Taiwan, Earthquake from a Realistic 3D Source and Crustal Structure. *J.*  
480 *Geophys. Res.*, **112**, B06307, doi: 10.1029/2006JB004615, 2007.

481 Lin, D.-H., Chen, H., Rau, R.-J., and Hu, J.-C.: The role of a hidden fault in stress  
482 triggering: Stress interactions within the 1935 Mw 7.1 Hsinchu–Taichung

483 earthquake sequence in central Taiwan, *Tectonophysics*. 37-52, doi:  
484 10.1016/j.tecto.2013.04.022, 2013.

485 Lu, W. T.: Seismicity Changes Prior to the M>6 Earthquakes in Taiwan During 1993  
486 to 2016 - an Approach of the RTL Algorithm. M.Sc. thesis, National Chung Cheng  
487 University, Taiwan, p 66, 2017. (in Chinese with English abstract)

488 Mignan, A., and Giovambattista, R. Di: Relationship between accelerating seismicity  
489 and quiescence, two precursors to large earthquakes. *Geophys. Res. Lett.*, **35**,  
490 L15306, doi:10.1029/2008GL035024, 2008.

491 Rau, R.J., Lee, J.C., Ching, K.E., Lee, Y.H., Byrne, T.B., and Chen, R.Y.: Subduction-  
492 continent collision in southwestern Taiwan and the 2010 Jiashian earthquake  
493 sequence. *Tectonophysics*, **578**, 107-116, doi:10.1016/j.tecto.2011.09.013, 2012.

494 Rundle, J.B., Klein, W., Turcotte, D.L., and Malamud, B.D.: Precursory seismic  
495 activation and critical point phenomena. *Pure Appl. Geophys.*, **157**, 2165-2182,  
496 doi:10.1007/PL00001079, 2000.

497 Simoes, M., Avouac, J.P., Beyssac, O., Goffe, B., Farley, K.A., and Chen, Y.G.:  
498 Mountain building in Taiwan: a thermokinematic model. *J. Geophys. Res.*, **112**.  
499 doi:10.1029/2006JB004824, 2007.

500 Shi, Y., and Bolt, B.A.: The standard error of the magnitude-frequency b value. *Bull.*  
501 *seism. Soc. Am.*, **72**, 1677-1687, 1982.

502 Shyu, J. B. H., Sieh, K., and Chen, Y.-G.: Tandem suturing and disarticulation of the  
503 Taiwan orogen revealed by its neotectonic elements. *Earth Planet. Sci. Lett.*, **233**,  
504 167-177, 2005a.

505 Shyu, J.B.H., Sieh, K., Chen, Y.-G., and Liu, C.-S.: Neotectonic architecture of Taiwan  
506 and its implications for future large earthquakes. *J. Geophys. Res.*, **110**, p. B08402,  
507 doi: 10.1029/2004JB003251, 2005**b**.

508 Sobolev, G.A., and Tyupkin, Y.S.: Low-seismicity precursors of large earthquakes in  
509 Kamchatka. *Volc. Seismol.*, **18**, 433-446, 1997.

510 Sobolev, G.A., and Tyupkin, Y.S.: Precursory phases, seismicity precursors, and  
511 earthquake prediction in Kamchatka. *Volc. Seismol.*, **20**, 615-627, 1999.

512 Suppe, J.: Kinematics of arc-continent collision, flipping of subduction, and backarc  
513 spreading near Taiwan. *Mem. Geol. Soc. China*, 21–33, 1984.

514 Wang, J.H.: The Taiwan Telemetered Seismographic Network. *Phys. Earth Planet.*  
515 *Inter.*, **58**, 9–18, 1989

516 Wang, J.H., Chen, K.C., and Lee, T.Q.: Depth distribution of shallow earthquakes in  
517 Taiwan. *J. Geol. Soc. China*, **37**, 125–142, 1994.

518 Wen, Y.-Y., Chen, C.-C., Wu, Y.-H., Chan, C.-H., Wang, Y.-J., and Yeh, Y.-L.:  
519 Spatiotemporal investigation of seismicity and Coulomb stress variations prior to  
520 the 2010 ML 6.4 Jiashian, Taiwan earthquake. *Geophys. Res. Lett.*, **43**,  
521 doi:10.1002/2016GL070633, 2016.

522 Wen, Y.-Y., and Chen, C.-C.: Seismicity variations prior to the 2016 ML 6.6 Meinong,  
523 Taiwan earthquake. *Terr. Atmos. Ocean. Sci.*, **28**, 737-742, doi:  
524 10.3319/TAO.2016.12.05.01, 2017.

525 Wu, Y. H.: An improved region–time–length algorithm applied to the 1999 Chi-Chi,  
526 Taiwan earthquake. M.Sc. thesis, National Central University, Taiwan, p 115,  
527 2006. (in Chinese with English abstract)

528 Wu, Y.M., and Chiao, L.Y.: Seismic Quiescence before the 1999 Chi-Chi, Taiwan, Mw  
529 7.6 Earthquake. *Bull. Seismol. Soc. Am.*, 96, 321-327, doi: 10.1785/0120050069,  
530 2006.

531 Wu, Y.M., Chen, C.-C., Zhao, L., and Chang, C.-H.: Seismicity characteristics before  
532 the 2003 Chengkung, Taiwan, earthquake. *Tectonophysics*, **457**, 177-182, doi:  
533 10.1016/j.tecto.2008.06.007.

534 Wu, Y.M., Chen, S. K., Huang, T.C., Huang, H.-H., Chao, W.A., and Koulakov, I.:  
535 Relationship between earthquake b-values and crustal stresses in a young orogenic  
536 belt. *Geophys. Res. Lett.*, **45**, 1832-1837, doi:10.1002/2017GL076694, 2018.

537 Wu, Y.M., Hsu, Y.J., Chang, C.H., Teng, L.S., and Nakamura, M.: Temporal and  
538 spatial variation of stress field in Taiwan from 1991 to 2007: Insights from  
539 comprehensive first motion focal mechanism catalog. *Earth Planet. Sci. Lett.*, **298**,  
540 306–316. <https://doi.org/10.1016/j.epsl.2010.07.047>, 2010.

541 Wyss, M., and Stefansson, R.: Nucleation points of recent mainshocks in Southern  
542 Iceland, mapped by b-values. *Bull. Seismol. Soc. Am.*, **96**, 599–608, 2006.

543 Yu, S.B., Chen, H.Y., and Kuo, L.C.: Velocity field of GPS stations in the Taiwan area.  
544 *Tectonophysics*, **274**(1-3), 41–59. [https://doi.org/10.1016/S0040-1951\(96\)00297-](https://doi.org/10.1016/S0040-1951(96)00297-1)  
545 [1](https://doi.org/10.1016/S0040-1951(96)00297-1), 1997.

546